

# External charge perturbation in a flowing plasma and electrostatic turbulence

Mridusmita Das<sup>a</sup> and Madhurjya P. Bora

*Physics Department, Gauhati University, Gwahati 781014, India.*

In this work, an 1D electrostatic *hybrid*-Particle-in-Cell-Monte-Carlo-Collision (*h*-PIC-MCC) code is used to study the response of a plasma to a moving, external, charged perturbation (debris). We show that the so-called pinned solitons can form *only* under certain specific conditions through a turbulent regime of the ion-ion counter-streaming electrostatic instability (IICSI). In fact, the pinned solitons are manifestation of the ion phase-space vortices formed around the debris. The simulation shows that the pinned solitons can form *only* when the debris charge density exceeds a certain value causing the counter-streaming ion velocity to exceed a critical velocity, pushing the instability to a turbulent regime. The effect of debris velocity is also essential for the appearance of pinned soliton as when the debris velocity increases, it causes the widening of the phase space vortices causing well-separated pinned solitons, which merge to form one single soliton when debris velocity reduces to zero. In the opposite extreme, when debris velocity becomes highly supersonic, the vortices are widened up to a limit causing the pinned solitons to disappear altogether. We further show the existence of a Kolmogorov-type energy cascade scaling for this electrostatic turbulence.

## I. INTRODUCTION

Despite being studied actively and widely since the days of Irving Langmuir (early 1920s), certain fundamental issues in plasma physics continue to enjoy the attention of the scientific community and prove their importance toward understanding the complex behavior of plasmas. In recent years, there has been a considerable interest in studying the response of a flowing plasma to an externally embedded charged perturbation (so-called debris), both theoretically [1–4] and experimentally [5–7]. One of the reasons for interest in this kind of problems is, in principle, exploring the possibility of detection of space debris in low-earth orbits (LEO) [1]. Historically, the effect of the movement of a charged particle through a plasma was studied quite a long time ago in 1955 [8]. Subsequently, several authors have studied the formation of wakes, generated by such movements in *e-i* as well as in complex plasmas [9–11]. The formation of wakes with reference to laser-plasma interaction was also studied by Malka and several others [12].

A localized charge perturbation in a plasma can primarily occur in two different ways – due to accumulation of charges on the surface of an external body such as debris which is embedded in the plasma and due to the formation of polarized structures as a result of self-consistent nonlinear interactions within the plasma itself [13]. In both the cases however, the charge perturbation, due to its localized nature, influences the plasma particles (both ions and electrons) in the neighborhood which can lead to the formation of nonlinear structures with interesting dynamics. One can find a number of theoretical works, which are devoted to the investigation of the formation of nonlinear structures due to external charge perturbations (debris) [1, 2, 4] theoretically as well as through molecular dynamics simulations [2, 3]. Several authors have also studied the effect of size and shape of these charged debris experimentally in the dust-acoustic regime using a complex plasma device [5, 7].

On the other hand, the self-organization of nonlinear structures in plasmas can give rise to Debye-scale polarized structure which can then act as a site of localized perturbation [13, 14]. With sufficient strength, these Debye-scale structures can give rise to streaming instabilities. An excellent review of these types of structures and their interactions can be found in a paper by Schamel [15]. In a recent work, Wang et al. [13] have carried out a statistical analysis of several bipolar electrostatic structures in the bow shock regions of Earth and argued that these bipolar structures [16] are ion phase-space holes produced by the two-stream instability triggered by the incoming and reflected ions in the shock transition region. These structures were detected by the *Magnetospheric Multiscale* (MMS) spacecraft [17].

Toward this, we in this work, explore the response of a plasma to a moving external charge perturbation through particle-in-cell (PIC) simulation. Particularly, we show that *only* a certain kind of charge perturbation leads to the formation of the so-called pinned solitons, which can be the manifestation of electrostatic turbulence, driven by an ion-ion counter-streaming instability (IICSI). The simulation itself is being carried out with our well-tested *hybrid*-PIC-MCC code [18–20]. However, we should be cautious to mention that in the *h*-PIC-MCC code, the Monte-Carlo collision algorithm is used only for collision of charged particles with dust particles, required for the purpose of charging of the dust particles. For all other cases, the simulation remains collision-less. Historically, two-stream instability by counter-streaming particles is quite well understood in the framework of kinetic theory [21–23]. They are also studied in the context of particle beam ramming through a plasma, both in classical and relativistic situations

---

<sup>a</sup> mridusmitadas1993@gmail.com

[24, 25]. However, there are a couple of fine points where we would like to draw the attention of the reader, especially the nonlinear saturation of the instability, where phase-space holes can sustain within a well-developed turbulence scenario [26]. In fact, in one of the works [27], it has been argued that ion-ion counter-streaming turbulence *cannot* possibly lead to the formation of electrostatic shocks, which also agrees with our simulation results.

In Section II, we review the basic theoretical framework for the formation of these Debye-scale structures triggered by the presence of charged debris [1, 4]. In Section III, we present our theoretical model (kinetic) for counter-streaming ion-ion instability and carry out a linear stability analysis for this particular situation. In Section IV, we present the results of our PIC simulation, which show the formation of dissipation-less shock waves (DSW) and pinned solitons for a charged external perturbation (debris). In Section V, we show how a negatively charged external perturbation can lead to a turbulent regime, only when the perturbation exceeds a certain threshold. Here, we show that the pinned solitons are basically a manifestation of the turbulent counter-streaming ion-ion instability. We also show that, not surprisingly, the turbulence has a Kolmogorov-type energy cascade scaling [28]. In this section, we estimate the minimum critical velocity required by the counter-streaming ion beams for sustaining the instability and compare it with our theoretical estimate. Toward the end, we have a short discussion on the effect of negatively charged dust particles on pinned solitons with results closely agreeing with other reported works [4]. Finally, in Section VI, we give a brief summary of our findings and concluding remarks.

## II. DEBYE-SCALE STRUCTURES IN A FLOWING PLASMA

In this section, we are going to briefly review the theoretical formalisms for different nonlinear Debye-scale structures, namely pinned solitons and DSWs in a flowing plasma. In order to investigate these nonlinear phenomena, we consider a 1D, collision-less  $e$ - $i$  plasma with an external charge perturbation (debris) of charge density  $\rho_{\text{deb}}$ . The debris charge density along with its shape and size are held constant throughout the simulation. The equations are continuity and momentum equations for ions, and Poisson's equation. The electrons can be considered to be inertialess in the ion-acoustic (IA) timescale,

$$\frac{\partial n_i}{\partial t} + \frac{\partial}{\partial x}(n_i v_i) = 0, \quad (1)$$

$$n_i \frac{dv_i}{dt} = -\sigma \frac{\partial n_i}{\partial x} - n_i \frac{\partial \phi}{\partial x}, \quad (2)$$

$$\frac{\partial^2 \phi}{\partial x^2} = n_e - n_i - \rho_{\text{deb}}, \quad n_e \sim e^\phi, \quad (3)$$

where electrons are assumed to be Boltzmannian. The above equations are expressed in normalized forms where we have expressed the ion pressure  $p_i = n_i T_i$ . The quantity  $\sigma = T_i/T_e$  and temperatures  $T_{i,e}$  are expressed in energy units. The charge density of the debris is denoted by  $\rho_{\text{deb}} \equiv \rho_{\text{deb}}(x - v_{\text{deb}}t)$ , which is moving with a velocity  $v_{\text{deb}}$ . We note that  $\rho_{\text{deb}} \leq 0$  depending on the nature of the debris charge. This model predicts the formation of pinned solitons [1] as well as DSWs [4] in the nonlinear regime under suitable conditions. In the above equations, the densities are normalized by their equilibrium values and electrostatic potential  $\phi$  is normalized by  $(T_e/e)$ . Length is normalized by electron Debye length and time is normalized by  $\omega_{pi}^{-1}$ , the inverse of ion plasma frequency. All velocities are normalized by the ion-sound speed  $c_s = \sqrt{T_e/m_i}$ .

We realize that depending on the nature and magnitude of  $\rho_{\text{deb}}$ , the response of the plasma can be quite different. While, for  $\rho_{\text{deb}} > 0$ , we might see the formation of DSWs in the precursor region, pinned solitons may form when  $\rho_{\text{deb}} < 0$ . Due to the presence of a strong accumulation of positive charge ( $\rho_{\text{deb}} > 0$ ), rapidly moving ions away from the debris site compresses the plasma in the precursor region which leads to the formation of DSWs. For sufficiently large  $\rho_{\text{deb}} < 0$ , IICSI may develop and results in an electrostatic turbulence, causing phase-space vortices to form which can effectively trap the ions spatially as well as temporally at the site of the debris. This trapping of ions is what causes the pinned solitons to form.

### A. Pinned solitons & DSWs

The formation of pinned solitons can be understood through the forced Korteweg-de Vries (fKdV) equation, which can be obtained following the well-established reductive perturbation analysis. To start with, we expand the variables  $g = (n_i, v_i, \phi, \rho_{\text{deb}})$  with respect to an expansion parameter  $\epsilon (\ll 1)$

$$g \sim \sum_{j=0,1,2,\dots}^{\infty} \epsilon^j g_j, \quad (4)$$

where  $g_0$  is the equilibrium value of the respective variables and  $g_j$ s are corresponding higher-order perturbations. The equilibrium ion velocity and plasma potential are assumed to be zero and the debris charge density is expected to contribute *only* at its second order  $\rho_2 \equiv (\rho_{\text{deb}})_2$  [1]. The stretched coordinates used in this case are

$$\zeta = \epsilon^{1/2}(x - v_{\text{ph}}t), \quad \tau = \epsilon^{3/2}t, \quad (5)$$

corresponding to the coordinate  $(x, t)$ , where  $v_{\text{ph}}$  is the phase velocity of the wave. Following the standard mathematics, an fKdV equation can be obtained [1] in the first-order perturbation in  $\phi$  as

$$\frac{\partial \phi_1}{\partial \tau} + \frac{1}{2} \left( \frac{\partial \phi_1^2}{\partial \zeta} + \frac{\partial^3 \phi_1}{\partial \zeta^3} \right) = \frac{1}{2} \frac{\partial \rho_2}{\partial \zeta}, \quad (6)$$

with  $\rho_2$  as a function of the stretched variable  $\zeta + (1 - v_{\text{deb}})t$ . It can now be shown that for a Gaussian-shaped debris potential  $\rho_{\text{deb}}(\zeta) \sim Ae^{-(\zeta/\delta)^2}$  with  $A < 0$  (negative charge perturbation), the above equation results in various kinds of pinned solitons [1], localized at the site of the perturbation. Note that the higher the value of  $\delta$ , the wider is the width of the debris charge distribution.

The above model can also be used to explain the formation of DSWs in ion density through the nonlinear Schrödinger equation (NLSE). The NLSE can be derived by using the same reductive perturbation theory but with a different set of stretched coordinates

$$\zeta = \epsilon(x - v_{\text{ph}}t), \quad \tau = \epsilon^2t, \quad (7)$$

and expansion of the variables  $g = (n_i, v_i, \phi, \rho_{\text{deb}})$  as

$$g(x, t; \zeta, \tau) = g_0 + \sum_{j=1}^J \epsilon^j \sum_{l=-L}^L g_{j,l}(\zeta, \tau) e^{il(kx - \omega t)}, \quad (8)$$

where  $v_{\text{ph}} = \omega/k$  is the phase velocity as before and the debris is supposed to contribute *only* in the second order. With these expansions, Eqs.(1-3) can be reduced to an NLSE or a Gross-Pitaevskii equation (GPE) in  $\phi_{1,1}$

$$i \frac{\partial \phi_{1,1}}{\partial \tau} + C_1 \frac{\partial^2 \phi_{1,1}}{\partial \zeta^2} + C_2 |\phi_{1,1}|^2 \phi_{1,1} = C_3 \rho_2 \phi_{1,1}, \quad (9)$$

with  $C_{1,2,3}$  as certain constants [4]. With the proper choice of  $\rho_2$ , the above equation can be solved in  $\phi_{1,1}$  or in ion density to show that it admits DSWs [4].

### III. COUNTER-STREAMING IONS AND PINNED SOLITONS

We note that the IICSI is the dominant one when the external charge perturbation is negative [13]. The saturation of IICSI is caused by ion-trapping and ion-heating, both of which depend on each other. Our simulations yield growth rates consistent with the linear theory and phase space structures. The electron-ion streaming instability is not relevant here as it is slower by one or more orders of magnitude than the IICSI. This is also revealed in earlier kinetic (Vlasov) simulation [29].

We now focus on the situation of what happens, when a Debye-scale structure (debris) of negative charge causes ions to counter-stream and ram into one another, causing an ion-ion two-stream electrostatic instability to develop and become turbulent when the debris charge is considerably large. We shall show that this turbulence caused by counter-streaming ion instability results in the formation of pinned solitons. In what follows, we shall build up a kinetic model for this to happen and follow it up with a PIC simulation.

#### A. Linear theory

Here, we are going to briefly describe the linear analysis of electrostatic instability in a plasma with equilibrium velocities in the framework of kinetic theory. Let us consider a multi-species, quasi-neutral, collision-less plasma with different species, having different equilibrium drift velocities. The basic governing equations are the electrostatic Boltzmann-Vlasov equations for different species and Poisson's equation for closure

$$\frac{\partial f_j}{\partial t} + \mathbf{u}_j \cdot \nabla f_j + \frac{q_j}{m_j} \mathbf{E} \cdot \frac{\partial f_j}{\partial \mathbf{u}_j} = 0, \quad (10)$$

$$\epsilon_0 \nabla \cdot \mathbf{E} = \sum_j q_j n_j, \quad (11)$$

where  $(f, \mathbf{u}, q, n)_j$  are the velocity distribution functions (VDFs), velocity, charge, and number density of the  $j$ th species respectively, and  $\mathbf{E}$  is the electric field. The VDF in general, can be expressed as a function of velocities and temperature for each species. For Maxwellian case, it becomes

$$f_j(u) \sim \exp \left[ -\frac{(u - v_j)^2}{2c_j^2} \right], \quad (12)$$

where  $v_j$  and  $c_j$  are the equilibrium drift velocity and thermal speed of the  $j$ th species, respectively,

$$c_j = (T_j/m_j)^{1/2}, \quad (13)$$

where the temperature is expressed in energy unit with  $T_j$  and  $m_j$  being the temperature and particle mass of the  $j$ th species. The quantity  $c_j$ , referred here as the thermal speed of species ' $j$ ' should not be confused with the ion-sound speed, which is denoted by  $c_s$ .

We now introduce a small electrostatic perturbation and express various physical quantities  $F$  with a linear perturbation scheme,  $F = F_0 + F_1$ , where  $F_{0,1}$  are equilibrium and perturbed parts. In our case

$$F = (f, \mathbf{E}), \quad F_1 \sim e^{-i\omega t + i\mathbf{k} \cdot \mathbf{r}}. \quad (14)$$

Further linear analysis of the above model leading to the linear dispersion relation is quite well-known [30] and the final dispersion relation can be written as

$$k^2 - \sum_j \omega_{pj}^2 \left( \mathbb{P} \int_{-\infty}^{+\infty} \frac{\hat{f}'_{j0}}{u_j - \omega/k} du_j + i\pi \hat{f}'_{j0} \Big|_{u_j=\omega/k} \right) = 0. \quad (15)$$

For clarity, a detailed analysis is given in Appendix A. Note that  $\hat{f}_{j0}$  is the unit-normalized velocity distribution function [see Eq.(A6)] and

$$\hat{f}'_{j0} = \frac{\partial \hat{f}_{j0}}{\partial u_j}. \quad (16)$$

The situation, we are particularly looking at is: when a negatively charged external perturbation (debris) is present in an  $e-i$  plasma, then from both sides of the debris there will be two counter-streaming ion populations moving towards the debris site and two counter-streaming electron populations moving away from it. However, in order to simplify the mathematics, we shall consider two drifting populations of ions with velocity  $\pm v/2$ . Besides, in order to eliminate kinetic effects of the electrons, we consider electrons to be Boltzmannian. Thus the ion VDFs are given by

$$\hat{f}_{i0}(u) = \frac{1}{\sqrt{2\pi c_i^2}} \left\{ \exp \left[ -\frac{(u + v/2)^2}{2c_i^2} \right] + \exp \left[ -\frac{(u - v/2)^2}{2c_i^2} \right] \right\}. \quad (17)$$

The above equation denotes two similar counter-streaming ion populations. As the debris charge is a symmetric Gaussian, the counter streams of ions are symmetric. The linearized Poisson's equation, Eq.(A3) becomes

$$ik\epsilon_0 E_{1x} = -en_{e1} + en_{i1}, \quad (18)$$

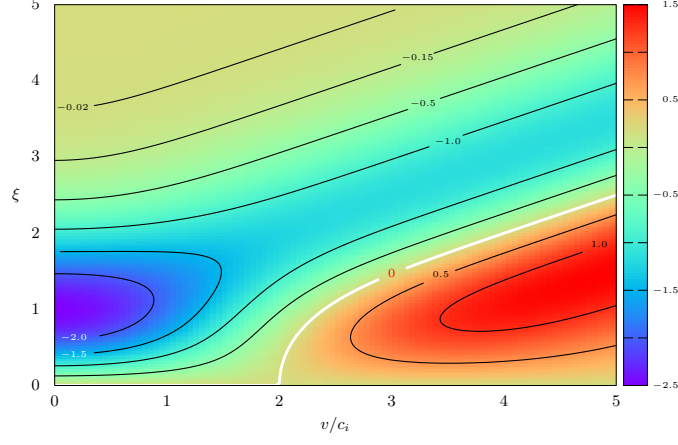
with

$$n_{e1} = n_0 \left( \frac{e\phi_1}{T_e} \right), \quad (19)$$

$$n_{i1} = \int f_{i1} d\mathbf{u}_i, \quad (20)$$

where  $f_{i1}$  is given by Eq.(A2). Eq.(19) is the linearized perturbed electron density, while the expression for electron density, in general, is given by

$$n_e = n_0 \exp \left( \frac{e\phi}{T_e} \right), \quad (21)$$

Figure 1. Contour plot of the function  $\mathcal{F}$ .

Substituting these expressions in Eq.(15), we have

$$k^2 = -\frac{1}{\lambda_{De}^2} + \frac{1}{2}\omega_{pi}^2 \left( \int_{-\infty}^{+\infty} \frac{F'(\tilde{u}^+)}{u - \omega/k} du + \int_{-\infty}^{+\infty} \frac{F'(\tilde{u}^-)}{u - \omega/k} du \right), \quad (22)$$

where we have substituted  $\phi_1 = iE_{1x}/k$  and

$$F(u) = \frac{1}{\sqrt{2\pi c_i^2}} \exp\left(-\frac{u^2}{2c_i^2}\right), \quad (23)$$

with  $\tilde{u}^\pm = u \pm v/2$ . Note that each ion population is responsible for half of the total ion density. Expressing  $u$  in terms of  $\tilde{u}$ , the integrations can be written as

$$\int_{-\infty}^{+\infty} \frac{F'(\tilde{u})}{\tilde{u} - \tilde{\omega}^\pm/k} d\tilde{u}, \quad (24)$$

where  $\tilde{\omega}^\pm = \omega \pm kv/2$  is the Doppler-shifted frequency. For small  $\text{Im}(u, \tilde{u})$ , one can approximate Eq.(22) as

$$k^2 = -\frac{1}{\lambda_{De}^2} + \frac{1}{2}\omega_{pi}^2 \left( \mathbb{P} \int_{-\infty}^{+\infty} \frac{F'(u)}{u - \tilde{\omega}^+/k} du + \mathbb{P} \int_{-\infty}^{+\infty} \frac{F'(u)}{u - \tilde{\omega}^-/k} du \right) + i\pi \frac{1}{2}\omega_{pi}^2 \left( \left. \frac{\partial F}{\partial u} \right|_{u=\tilde{\omega}^+/k} + \left. \frac{\partial F}{\partial u} \right|_{u=\tilde{\omega}^-/k} \right). \quad (25)$$

Proceeding as before, we can estimate the growth rate of the instability as

$$\text{Im} \left( \frac{\omega}{\omega_{pi}} \right) \simeq \frac{1}{4} \sqrt{\alpha^3 \pi} \left( \frac{\omega_{pi}}{kc_i} \right)^3 \tilde{\omega}_{pi} \left\{ \left( \frac{kv}{2\omega_{pi}} - 1 \right) \exp \left[ -\frac{(\omega_{pi} - kv/2)^2}{2k^2 c_i^2} \right] - \left( \frac{kv}{2\omega_{pi}} + 1 \right) \exp \left[ -\frac{(\omega_{pi} + kv/2)^2}{2k^2 c_i^2} \right] \right\}, \quad (26)$$

where  $\alpha$  is a dimensionless parameter defined in Eq.(B5). The detailed analysis leading to the derivation of the above relation is given in Appendix B.

## B. Critical velocity

Normalizing  $v \rightarrow v/c_i$  and  $\gamma = \text{Im}(\omega/\omega_{pi})$ , one can conveniently express Eq.(26) as

$$\gamma = \frac{1}{8} \tilde{\omega}_{pi} \xi^2 \sqrt{\pi \alpha^3} \mathcal{F}, \quad (27)$$

where  $\tilde{\omega}_{pi}$  is a dimensionless ion plasma frequency as defined in Eq.(B6) and

$$\mathcal{F} = (v - 2\xi) \exp\left[-\frac{(v/2 - \xi)^2}{2}\right] - (v + 2\xi) \exp\left[-\frac{(v/2 + \xi)^2}{2}\right] \quad (28)$$

with  $\xi = 1/(k\lambda_{Di})$  and  $\gamma$  as the normalized growth rate, the sign of which is determined by  $\mathcal{F}$ . A contour plot of the term  $\mathcal{F}$  is shown in Fig.1. As shown in the figure, one can find out the minimum critical velocity  $v_c$  of the ion streams required to excite the instability ( $\gamma > 0$ ) can be calculated from the curve  $\mathcal{F} = 0$  by seeking the minimum  $v$ . However, solutions of the equation  $\mathcal{F} = 0$  can only be expressed in terms of inverse functions and in general one cannot obtain a full spectrum of solutions including the equation for the curve of minimum  $v$  (the white curve in Fig.1). One can, however, obtain  $v_c$  by expanding  $\mathcal{F}$  around  $\xi = 0$  and find the solution of the resultant equation after setting  $dv/d\xi = 0$  as,

$$(v_c^2 - 4) e^{-v_c^2/8} = 0, \quad (29)$$

which yields  $v_c = 2$ . In terms of ion-sound speed  $c_s = \sqrt{T_e/m_i}$ ,  $v_c \simeq 2\sqrt{\sigma}c_s \sim 0.63c_s$  for  $\sigma = 0.1$ , which is quite within the limit  $c_s > v_c > 1.3c_i$  [23]. For a situation when external charge perturbation (i.e. debris) is stationary relative to the plasma, it is the debris potential which causes acceleration of the ions. The maximum velocity  $v_{\max}$  an ion can obtain for a potential difference of  $\varphi$  between the debris and bulk plasma can be found by equating the electrostatic energy to the kinetic energy of the ions  $v_{\max} = (2ef\varphi/m_i)^{1/2}$ , where  $f$  is the fraction of electrostatic energy that is converted to the kinetic energy of the ions, which lies between 0 and 1 and  $e$  is the electronic charge. Normalizing the potential by  $(T_e/e)$  and velocity by  $c_s$ , we find  $\phi = v_{\max}^2/(2f) \sim 2\sigma f^{-1}$ . Usually, when we consider the acceleration of charged particles through an electrostatic potential drop, we consider the source of the potential to be infinitely large so that all particles get accelerated equally. However, in this case, when an ion is accelerated by the debris potential, it will reduce the potential for the subsequent particles and the effective potential available for incoming particles will be continuously reduced, which is being taken care of by the factor  $f$ , much like Debye shielding.

At this point, we should also note that the magnitude of  $v_c$  is directly related to the  $\rho_{\text{deb}}$  in the sense that the higher is the value of  $\rho_{\text{deb}}$ , the larger is the value of  $v_c$ . So, a higher  $\rho_{\text{deb}}$  should quickly trigger the instability while for a smaller value of  $\rho_{\text{deb}}$ , the perturbation causing the instability should be completely thermalized. We can see this effect when we discuss the onset of turbulence in Section V, where we can see that there exists a critical value of  $\rho_{\text{deb}}$  beyond which only turbulence can set in.

#### IV. PIC SIMULATION

We now perform a PIC simulation of a 1-D  $e$ - $i$  plasma with positively and negatively charged debris. We shall see the formation of DSWs for a strong positively charged external perturbation (debris) and how the turbulence caused by counter-streaming ions due to a negatively charged external perturbation (debris) gives rise to pinned solitons. The PIC code used in these simulations is the  $h$ -PIC-MCC code, which can simulate plasma processes in the IA, dust-ion-acoustic (DIA), and electron time scales with dust-charge fluctuation. More about this code and its benchmarking results can be found in the papers by Changmai and Bora [18, 19] and Das et al. [20].

In our simulation, the simulation box length is 0.006 m, where both electrons and ions are represented each with  $10^5$  computational particles with an ion-to-electron mass ratio of 1836. The simulation box is divided into grid of 600 uniform cells. For the plasma parameters used in this simulation (please see the next subsection), the electron Debye length comes out to be  $\lambda_D \sim 7.4 \times 10^{-5}$  m and the electron plasma frequency  $\omega_{pe} \sim 5.9 \times 10^9$  rad/s. We use a numerical evolution time step  $\sim 10^{-11}$  s. With these simulation parameters, we are able to have full temporal resolution at electron timescale and spatial resolutions over the entire simulation domain. In our simulation, we have distributed the electrons and ions with their respective Maxwellian velocity distributions [31]. This results in a linear Poisson's equation Eq.(3), which is solved with successive over-relaxation (SOR) method. The simulation is being run with periodic boundary conditions.

##### A. Formation of DSW

The results of this PIC simulation of this model of an  $e$ - $i$  plasma are shown in Fig.2 (this study), which shows the formation of DSW when  $v_{\text{deb}} \geq c_s$  for  $\rho_{\text{deb}} > 0$ , where  $v_{\text{deb}}$  is the debris velocity w.r.t background plasma and  $c_s = \sqrt{T_e/m_i}$  is the ion-sound speed with temperature expressed in energy units. The debris is a Gaussian-shaped

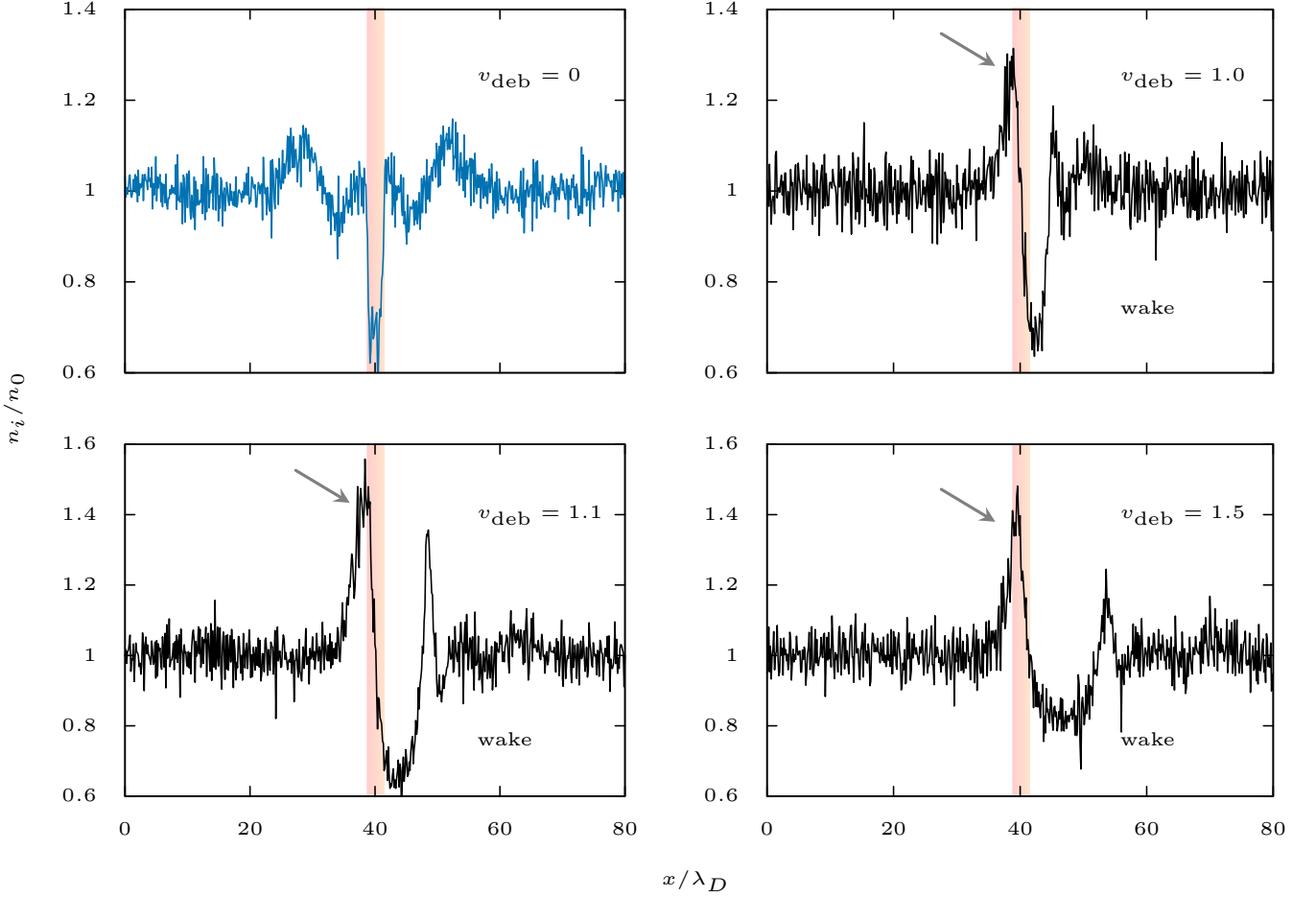


Figure 2. Formation of DSW in ion density due to a positive external charge perturbation. The vertical colored stripe, in each panel, indicates the position of the Gaussian shaped positive charge debris. The arrows indicate the DSW structure as the debris moves from right to left with velocity  $v_{\text{deb}}$  (normalized by ion-sound speed  $c_s$ ). For a static perturbation, what we see is the propagation of an IAW from the site of initial perturbation, which changes to a DSW as velocity increases. The figures are in the rest-frame of the debris.

charge distribution with width  $\sim \lambda_D$ , which is of the order of a few Debye lengths, shown as an orange-colored strip in Fig.2. The relevant plasma parameters in this case are as follows: plasma number density  $n_i \sim n_e = 10^{16} \text{ m}^{-3}$ , electron temperature  $T_e = 1 \text{ eV}$ , ion temperature  $T_i = 0.01 \text{ eV}$ , and  $|\rho_{\text{deb}}| \sim 0.09\rho_0$  without taking into account the background plasma density and  $\rho_0 = en_{i,e}$  is the equilibrium plasma density and  $e$  being the value of electronic charge. All figures are drawn in the rest-frame of the debris. The plasma parameters used in this simulation work can be representative of space plasma such as found in low-Earth orbit (LEO) plasma, though we have used a relatively higher plasma density so as to enhance the effect of debris (external charge perturbation) according to  $|\rho_{\text{deb}}| \sim 0.09\rho_0$  for more clear observation of the debris effect. Note that the instability growth rate  $\gamma \propto \tilde{\omega}_{pi}$ , the re-defined ion-plasma frequency which essentially implies that  $\gamma \propto n_i^{1/2}$ . So the lower is the plasma density, the lower is the growth rate and instability will take a longer time to develop. By using a bit higher plasma density we can make the effect of the instability visible quickly without compromising other physical effects. As the primary objective of this work is to understand the physics of different nonlinear structures formed due to the presence of external charged debris, we use the results of work as a ‘proof of principle’. So, the results presented are general in nature and are expected to enrich the general understanding of such situations rather than exactly explaining specific details of any particular situation. For example, similar phenomena are experimentally observed in laboratory plasmas, the parameters for which are representative of the earth’s bow shock region [5].

As can be seen from the figure, for a static debris, the perturbation results in the formation of IAW, which propagates away from the site of the debris, while a dispersive (oscillating) shock front appears on the front of the debris with an IA wake when there is a relative velocity between the plasma and the debris. These results are in good agreement with fluid simulation results, as reported by Sarkar and Bora [4], which also provides a purely theoretical explanation

of these oscillations in terms of nonlinear Schrödinger equation (NLSE) in the plasma potential  $\phi$  [4].

### B. Formation of pinned solitons

In this section, we present the results of our PIC simulation and show how a localized counter-streaming ion instability can form, sustain and gives rise to the formation of pinned solitons through electrostatic turbulence. We shall also see how the simulation results closely agree with our theoretical analysis (for the linear regime), as already described in Section III.

The results of this simulation are shown in Fig.3, in which we plot the ion density  $n_i$  as well as the scatter plot of the ion phase-space for various  $v_{\text{deb}}$  for a negative charge perturbation ( $\rho_{\text{deb}} < 0$ ) in the rest frame of the debris, which is centered in the simulation box at  $\sim 40\lambda_D$ . What we observe is a *localized* acceleration of ions by the negatively charged debris potential causing a counter-streaming ion instability to develop which then goes on to the nonlinear saturation regime, ultimately entering a turbulent regime. The left panels in the figure show the ion density, which are the pinned solitons, resulted by trapping of ions in the phase space vortices. We further see that as debris velocity increases, it causes the widening of the vortices causing well-separated pinned solitons. In the limit of  $v_{\text{deb}} \rightarrow 0$ , the single soliton that we can see is nothing but the merger of multiple pinned solitons. This is evident from the fact that as debris velocity increases, the vortices get widened and the solitons are un-merged which ultimately gets separated. One can also see that this un-merging causes the heights of the final solitons to decrease due to redistribution of the energy, originally contained in a single soliton only (see Fig.3, the heights of the solitons are marked for easy reference). It should, however, be noted that this is distinctly different from the situation where two independent solitons approach and cross each other, making the composite soliton height increase momentarily during the cross over. In our case, the multiple solitons un-merge into separate solitons. However, when  $v_{\text{deb}} \gg c_s$ , the vortices are widened up to a limit where pinned solitons cannot form. This is primarily due to the fact that ‘free’ (linear) perturbations will not move faster than  $c_s$ . So, pinned solitons can form *only* within a window of range of debris velocities. These results are consistent with the findings of Tiwari [2] and Sarkar [4]. At this point, we would also like to emphasize that DSWs can possibly form with positively charged debris or in other words the IICSI *cannot* be responsible for the formation of any shock structure, which also agrees with an earlier study [27].

It will be interesting to compare these extremely localized counter-streaming instabilities to the classical streaming instability. In the usual case of streaming instability, the entire ion population rams into one another and vortices form all over the domain, whereas in a charged debris-induced case, as we have seen, the instability is severely localized, only in the neighborhood of the debris, which causes the pinned solitons to form. In Fig.4 (left panel), we show the formation of such an instability and the electrostatic energy history of the plasma (in terms of potential energy density  $u_{\text{pot}}$ ), which shows the linear growth of the instability.

The linear growth is marked by the exponential rise of the electrostatic energy, followed by a quasilinear stage and nonlinear saturation. The linear growth rate in this case is  $\gamma \sim 0.15$ . In this case, the initial kinetic energy of the counter-streaming ions is converted to electrostatic potential energy as the instability grows. The streaming velocity of the ions with respect to their counter-streaming part is  $\sim 3c_i$ .

On the other hand, in the debris-induced streaming instability, the electrostatic potential energy of the debris is converted to the kinetic energy of the accelerating ions, which is then converted back into the electrostatic potential energy of the ions as they become trapped in the phase space vortices. This evolution of kinetic energy is shown in the right panel of Fig.4. Note that the decrease of kinetic energy is at the cost of increasing electrostatic energy which is depicted by the decay curve of the kinetic energy. In this case, we have chosen to plot the kinetic energy as the instability is extremely localized. We note that in PIC simulation, the electrostatic potential is interpolated at the grid points, which makes it usually difficult to find the localized contributions of the instability to the increase in potential energy. However, as the kinetic energy is calculated at the particle positions, it is rather easier to calculate the kinetic energy for particles confined within a region and is a good marker of the underlying instability. The situation however is different in the case of a non-localized streaming instability, where the potential and kinetic energies of the entire population of the plasma particles get evolved, such as one shown in the left panel of Fig.4. In this case, one can use either potential or kinetic energy to keep track of the instability. Also note that the physical and computational models do not have any dissipative effects, making the system fully conservative and one can use either potential or kinetic energy, depending on the ease of use. The instability growth rate in the debris-driven case is found to be  $\gamma \sim 0.13$ , corresponding to the topmost plot in Fig.3 where the debris velocity w.r.t the background plasma is zero. The effective counter-streaming velocity of the ions towards the debris site in this case is  $\sim 5.6c_i$ , which is almost twice the value needed for classical IICSI for the equivalent growth rate. This can be understood from the extremely localized nature of the instability. As the plasma away from the site of perturbation (debris) is *not* affected, the surrounding plasma tends to thermalize the perturbation requiring a higher streaming velocity to sustain the instability. It is also obvious why these events are extremely localized, which is due to the Debye shielding



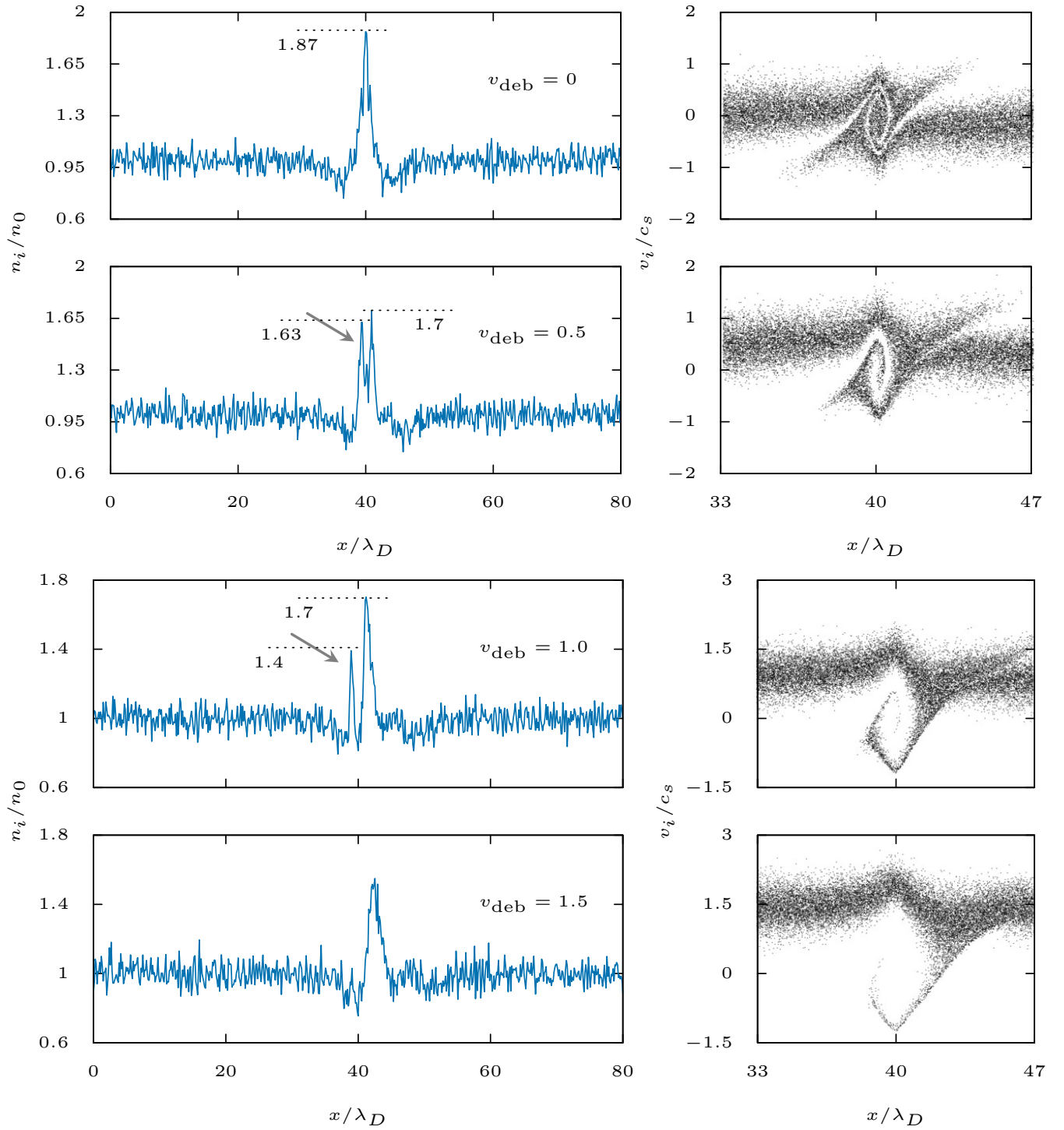


Figure 3. Formation of pinned solitons due to a negative external charge perturbation at the debris site for different debris velocity  $v_{\text{deb}}$  (normalized by ion-sound speed  $c_s$ ). In the figure, we have shown the ion density  $n_i$  (left panel) and the corresponding phase-space for the pinned solitons, showing phase-space vortices, indicating electrostatic turbulence (right panel). The arrow shows the pinned solitons. Pinned solitons cease to form at higher  $v_{\text{deb}}$  (lower panel).

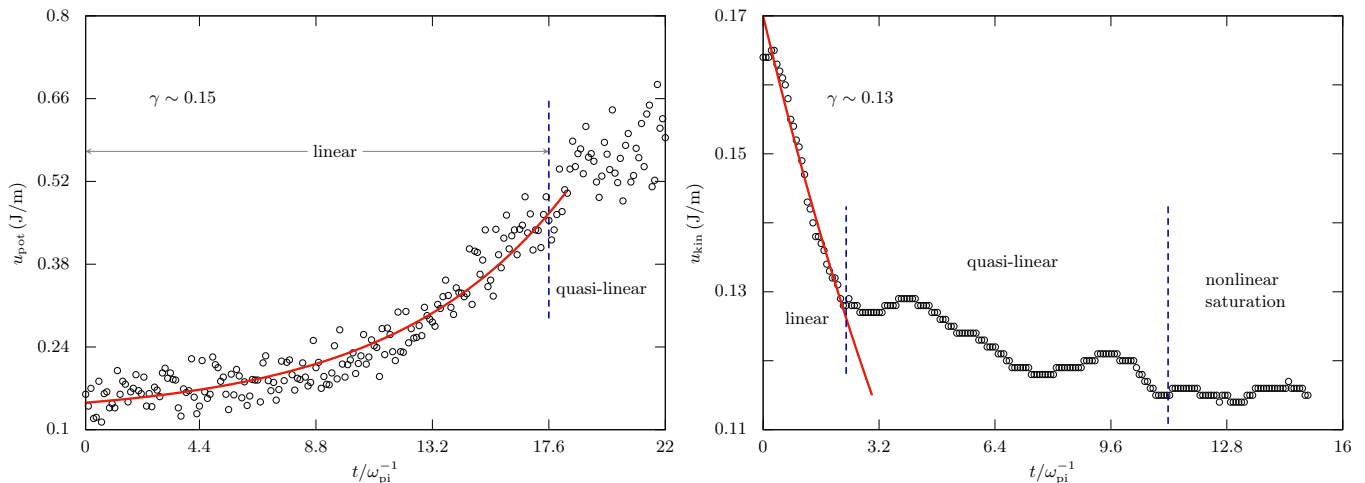


Figure 4. Potential (left) and kinetic (right) energy histories of the classical counter-streaming ion (left) and debris-driven ion instabilities (right). Both plots show energy densities as the instabilities develop. While the open circles show the respective simulation data, the solid lines show the exponential rise (decay) of the potential (kinetic) energies during the linear regime of the instability. The other regions are marked accordingly.

of the disturbance caused by debris.

Before we proceed further, we would like to discuss the exact nature of external charged debris in a flowing plasma. In situations such as LEO, charged debris may arise due to the presence of different kinds of so-called foreign objects such as parts of de-commissioned and broken parts of satellites, collectively referred to as ‘space debris’ [32]. These debris may get charged due to different reasons [33–38] including photoemission of electrons as a result of exposure to high energy solar radiation [39]. We should also note that the cumulative amount of charge of a debris is not expected to remain constant in time but should vary with different timescales and may also have a stochastic component of variability as well [40]. However, modeling such variations is extremely difficult as we do not have enough first-hand experimental data on such variations. This is why, in all such work dealing with external charged debris in flowing plasmas, it is customary to treat the debris charge as constant in time. In this PIC simulation also, we have treated the cumulative charge and shape of the debris constant in time. Dynamically, a PIC plasma simulation is quite closer to a realistic physical process, so long as the plasma is not strongly coupled. So, when an external debris is introduced into a plasma, the surrounding plasma will try to neutralize the excess charge, much like a Debye shielding effect, as already mentioned in Section III. In the absence of any relative velocity between the debris and the bulk plasma, the localized disturbance created by the charged debris is expected to thermalize as time progresses. For the parameters used in this simulation, we see that the fastest ion-acoustic time scale  $\tau_{IA} \sim (kc_s)^{-1}$ , assuming the largest  $k \sim 2\pi/(10\lambda_D)$  with  $10\lambda_D$  as the average size of debris, is of the same order as the ion plasma timescale  $\tau_{pi}$ . On the other hand, the IICSI growth rate is quite slower  $\sim 0.1\omega_{pi}$  and the thermalization time should be about several order magnitudes higher than the IICSI timescale. As a result, when there is a relative velocity and the debris becomes a moving object and the localized disturbance never gets time to thermalize, as by the time the instability builds up, the debris moves ahead and the IICSI continues to build up keeping the structures sustained in time, which is what we have seen in the simulation.

## V. ONSET OF TURBULENCE

We shall now try to see the onset of turbulence due to an external charge perturbation or debris. However, an interpretation of 1D turbulence is in order here. Heuristically, any discussion on turbulence essentially leads to Kolmogorov’s 1941 work [28], which provides a scaling on energy cascades in an inertial subrange

$$E(k) \sim \varepsilon^{2/3} k^{-5/3}, \quad (30)$$

where  $E(k)$  is the turbulent energy density,  $k$  is the wave number, and  $\varepsilon$  is the energy available for the fluid per unit mass and time. Alternatively,  $\varepsilon$  can also be interpreted as the energy which cascades from scale to scale and gets dissipated by viscosity beyond the inertial subrange. However, the above scaling is true strictly for a three-dimensional situation whereas our observation is for a dissipation-less 1D case with dispersion. Therefore, we identify our case

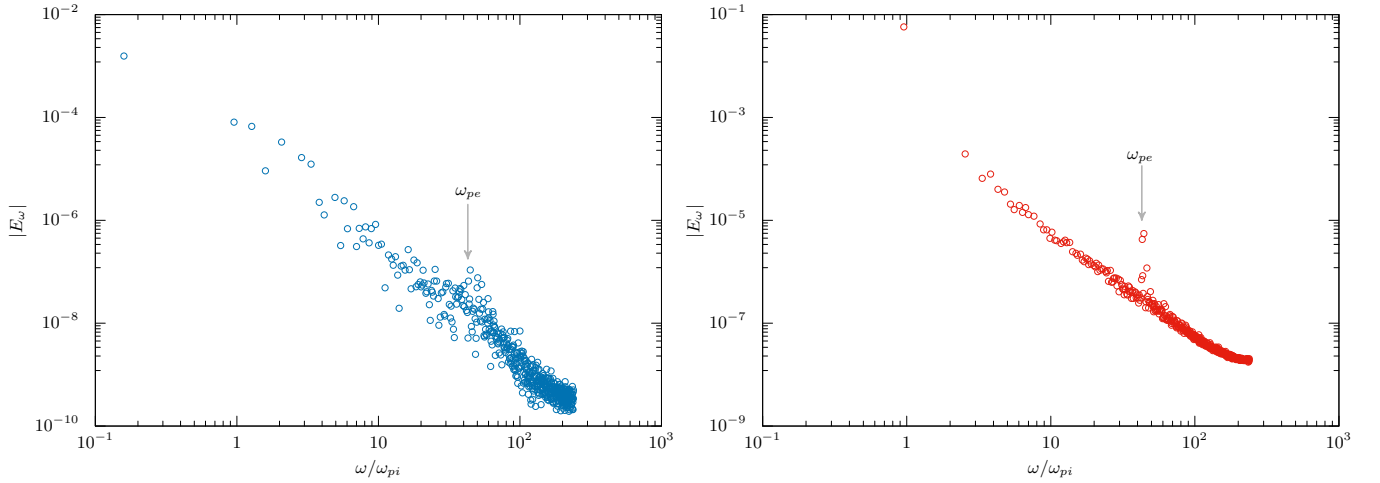


Figure 5. The power spectrum density (PSD) for random fluctuations (left) and a fully developed turbulence (right).

with the basic and well-known 1D turbulence model by Majda, McLaughlin, and Tabak [41] (thereafter MMT) which describes the 1D turbulence for dispersive wave with the help of a family of dynamical equations [42]

$$i \frac{\partial \psi}{\partial t} = \left| \frac{\partial}{\partial x} \right|^\eta \psi + \lambda \left| \frac{\partial}{\partial x} \right|^{\beta/4} \left( \left| \frac{\partial}{\partial x} \right|^{\beta/4} \psi \right)^2 \left| \frac{\partial}{\partial x} \right|^{\beta/4} \psi, \quad \lambda = \pm 1, \quad (31)$$

where  $\psi(x, t)$  is a complex wave field and  $(\eta, \beta)$  are real parameters. For  $\eta = 2$  and  $\beta = 0$ , the above equation reduces to an NLSE, as given by Eq.(9), which is also as in our case. Eq.(31) conserves two integrals, namely  $L^2$ -norm (wave action) and momentum

$$\int |\psi|^2 dx, \text{ and } \int (\psi \bar{\psi}_x - \psi_x \bar{\psi}) dx, \quad (32)$$

respectively, where the subscript denotes spatial partial derivative and the  $\bar{\psi}, \bar{\psi}_x$  denote the corresponding complex conjugates. Kolmogorov-type energy scaling laws are basically the equilibrium solutions of the model, namely [41, 42]

$$\tilde{n}(\omega) \sim \omega^{(-2\beta/3-1+\eta/3)/\eta}, \quad (33)$$

$$\tilde{n}(\omega) \sim \omega^{-(2\beta/3+1)/\eta}, \quad (34)$$

where the quantity  $\tilde{n}$  can be interpreted as the spectral density of the wave field in  $\omega$ -space. Apart from these one-dimensional energy scaling, the resultant NLSE can also support solitons and quasi-solitons (solitons with finite lifetime) [42]. For the parameter  $\lambda = -1$ , the NLSE is known as focusing NLSE, which can support solitons and quasi-solitons [42].

Following the above discussion, we now argue that the power spectrum of the turbulent energy density in the debris-induced streaming instability should follow similar laws like relations (33,34). Apparently, we can estimate the parameters  $(\eta, \beta)$  from our obtained scaling. Computationally, in order to quantify the onset of turbulence, we plot the power spectrum density (PSD)  $|E_\omega|$  of the kinetic energy, against frequency  $\omega$ . Here,  $E_\omega$  is obtained through the Fourier transformation of the total kinetic energy  $E(t)$ . The results are shown in Fig.5. In the figure, we have shown the PSDs – one for random fluctuations in the plasma when no particular perturbation is present (left panel) and one when an external negative charge perturbation is introduced, resulting in a fully developed turbulence (right panel). As is evident from the figure, we can clearly see a Kolmogorov-type scaling in the right panel, signifying turbulence. The relevant parameters for a 1D plasma are as follows: the equilibrium plasma density  $n_0 \sim 10^{16} \text{ m}^{-3}$  and electron temperature  $T_e \sim 1 \text{ eV}$  with  $\sigma = 0.01$ . Assuming that a fully developed turbulence results in a Kolmogorov-type scaling, we try to detect the onset of turbulence by estimating the deviation of the PSD from that of Kolmogorov-type scaling, when the strength of the external charge debris exceeds a certain threshold. The PSDs shown in these figures are due to the turbulence energy density measured when the turbulence is fully developed and the instability reaches a nonlinear saturation regime (unless otherwise stated), corresponding to the ‘third region’, shown in the second panel of Fig.4.

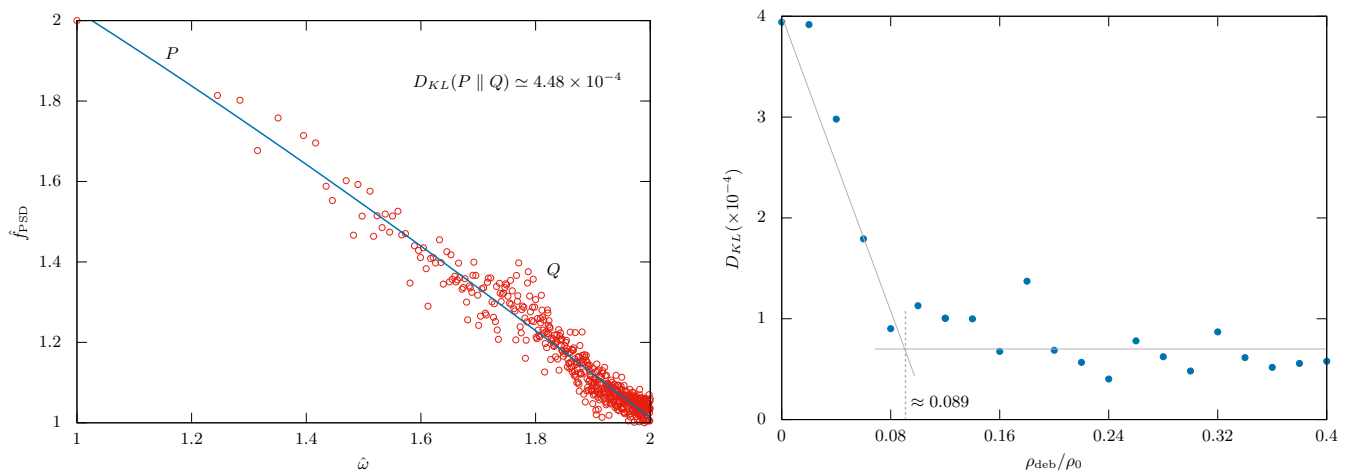


Figure 6. The divergence  $D_{KL}(P \parallel Q)$  for random fluctuation is shown in the left panel. Note that both the axes are normalized to the interval  $[1, 2]$  with a suitable normalized frequency  $\hat{\omega}$ . A plot of  $D_{KL}(P \parallel Q)$  versus external charge density  $\rho_{\text{deb}}$  normalized to equilibrium charge density is shown in the right panel. The sudden change of behavior of  $D_{KL}(P \parallel Q)$  signifies the onset of turbulence. The threshold value of  $\rho_{\text{deb}}$  required to sustain the instability is found to be  $\sim 0.089$ , which is very close to the theoretically estimated value.

In order to carry out the computational analysis, we estimate the so-called *divergence* of a dataset for PSD from the ideal one (Kolmogorov-type) by calculating the relative entropy, also known as Kullback–Leibler divergence, denoted as  $D_{KL}(P \parallel Q)$ . This method treats the datasets as distributions  $P$  (considered as an ideal power-law distribution) and  $Q$  (PSD distribution obtained from simulation) and estimates the divergence of the target distribution  $Q$  from the sample distribution  $P$ . The lower is the value of the divergence, the more closer is the distribution  $Q$  to  $P$ . To start with, we generate the ideal Kolmogorov-type distribution  $P$  by fitting the following nonlinear function to the distribution  $Q$ ,

$$P \equiv \hat{f}_{\text{PSD}} = a + bp^c, \quad (35)$$

in the log-log space. In the above fitting,  $p$  denotes a point on the PSD spectrum and  $a, b, c$  are fitting constants. This fitting is inspired by the Kolmogorov-type cascading power law. It is to be noted that in order to avoid complex singularity in the dataset, we have normalized the target dataset to a positive definite interval of  $[1, 2]$  on both axes, although in principle one can normalize it to any arbitrary interval. We note that the normalization is usually desirable to avoid simultaneous appearance of both large and small numbers, as with any other computational methods. The results of the analysis are summarized through Fig.6, where we have shown the calculation of this divergence for random fluctuation (left), for which  $D_{KL}(P \parallel Q) \simeq 4.48 \times 10^{-4}$ . On the right panel, we have plotted the divergence  $D_{KL}(P \parallel Q)$  for various negative debris charge density  $\rho_{\text{deb}}$  (external perturbation). From the figure, what we see is a sudden shift in the value of the divergence from a linear decreasing trend to a near-constant state, signifying the onset of turbulence. The point of onset can be found from the intersection of the two curves as shown in the figure, which comes out to be  $|\rho_{\text{deb}}| \sim 0.09$ , normalized to the equilibrium charge density which is unity. The random fluctuations represent the energy cascade when no specific perturbation is present. Since, a minimum critical velocity  $v_c$  is required for the counter-streaming ions for the IICSI to develop, the magnitude of  $v_c$  is however dependent on  $\rho_{\text{deb}}$  in the sense that a minimum  $\rho_{\text{deb}}$  is required to make  $v_c$  exceed that critical value. Once  $\rho_{\text{deb}}$  is beyond this threshold, then the higher is the magnitude of  $\rho_{\text{deb}}$ , the quicker  $v_c$  attains its value, and the quicker the IICSI develops.

The minimum critical velocity of the counter-streaming ions required to sustain a turbulent regime deserves some comments before estimating it. We should note that the critical velocity (of counter-streaming ions) estimated through the linear analysis in Section III-B is the one which is needed for the instability to grow. However, when the counter-streaming instability is induced by a negative external charge perturbation, as we have seen, the instability is highly localized. For the instability to grow linearly and reach a nonlinear saturation, it has to compete against the thermal fluctuations of the surrounding plasma, before the latter can overwhelm the instability. Naturally, it requires a higher critical velocity for the instability to be sustained.

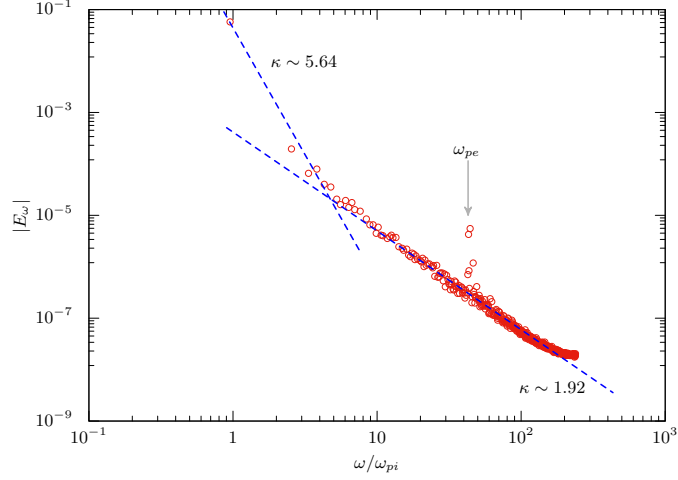


Figure 7. Kolmogorov-type power law ( $E_\omega \propto \omega^{-\kappa}$ ) for the ion-ion counter-streaming electrostatic turbulence.

### A. Estimating $v_c$ from the simulation

We now estimate the critical velocity required by counter-streaming ions to develop and sustain the instability as indicated previously. Consider the normalized 1D Poisson's equation for debris

$$\frac{d^2\phi}{dx^2} = \rho_{\text{deb}}(x), \quad (36)$$

where  $\rho_{\text{deb}}(x)$  is the debris charge density, which is a very steep-flat Gaussian-shaped, just like a top-hat function

$$\rho_{\text{deb}}(x) = \rho_{\text{peak}} e^{-\varrho x^{2\nu}}, \quad (37)$$

where  $\rho_{\text{peak}}$  is the value of the peak charge density (unsigned) at  $x = 0$ ,  $\varrho$  is a positive constant which essentially determines the spread (width) of the charge distribution, and  $\nu$  is a large positive integer which determines the *steepness*. Note that here we have used a generalized expression for the symmetric debris charge profile, though in the simulation we have used a pure Gaussian profile. The potential should also be symmetric around the middle point. In the extreme case,  $\rho_{\text{deb}}(x)$  becomes a top-hat function which can be represented with a Heaviside step function  $H(x)$

$$\rho_{\text{deb}}(x) = \rho_0 [1 - H(|x| - \varrho)]. \quad (38)$$

Eq.(36) can then be solved analytically with the boundary condition  $(\phi, \phi')|_{x \rightarrow z} = 0$  with  $z > \delta L$ , where  $\delta L$  is the length over which the debris charge is spread out. The solution for  $\phi_0$  for the form of  $\rho_{\text{deb}}$  given by Eq.(37), can be written in terms of the exponential integral  $\text{Ei}_\mu(z)$  with

$$\phi_0 \equiv \phi|_{x=0} = \frac{\rho_0}{2\nu} z^2 \text{Ei}_\mu(\varrho z^{2\nu}), \quad \mu = 1 - \frac{1}{\nu}, \quad (39)$$

where  $\phi_0$  is the value of the potential at the center of charge perturbation and  $\text{Ei}_\mu(z)$  is defined as

$$\text{Ei}_\mu(z) = \int_1^\infty t^{-\mu} e^{-zt} dt, \quad \text{Re}(z) > 0. \quad (40)$$

The numerical weight  $w$  (which is the actual number of real plasma particles represented by one computational particle) for the debris in the PIC simulation is same as for electrons, as debris can be thought to be a collection of electrons in this case. As such

$$w = n_0 L / N, \quad (41)$$

where  $n_0$  is the equilibrium plasma density  $\sim 10^{16} \text{ m}^{-3}$ ,  $L$  is the simulation box length which is 0.006 m, and  $N$  is the number of computational particles which is  $10^5$ . These parameters yield  $w \simeq 6 \times 10^8$ . So, the debris charge density  $\rho_{\text{deb}}$  can be written as

$$\rho_{\text{deb}} \sim \frac{Q_{\text{deb}}}{\delta L}, \quad (42)$$

where  $Q_{\text{deb}} = ewN_{\text{deb}}$ . From our simulation, we have found that we need about  $N_{\text{deb}} \sim 800$  number of excess computational particles to simulate the debris with  $\delta L \sim (5 - 10)\lambda_D$ , required for the instability to develop and sustain. With this, we can estimate the peak charge density  $|\rho_{\text{peak}}| \sim 0.08$ , normalized to the equilibrium charge density  $\rho_0 = |en_0|$ , without taking account of the background plasma density. This value can be compared with the numerically obtained one  $\sim 0.089$ , to which it indeed agrees very closely.

As the potential has to be symmetric around the midpoint ( $x = 0$ ), for  $\varrho$  we can take only half of the width of the charge distribution starting from its middle, i.e.  $\delta L/2$  and can estimate from Eq.(39) that  $|\phi_0| \sim 0.16$ . Assuming that this peak potential to be responsible for ion acceleration, the critical velocity can be calculated as

$$v_c = \sqrt{2|\phi_0|} \simeq 0.57. \quad (43)$$

Note that the above value is normalized to the ion-sound speed  $c_s = \sqrt{T_e/m_i}$ , which when normalized by the ion thermal velocity, becomes  $\sim 5.65$  for  $\sigma = 0.01$  for which the simulation is being run. As we have already discussed, the theoretical value calculated from the linear theory comes out to be 2 (see Section III-B), which is lower than what is obtained from the simulation. This discrepancy can be justified considering the fact that the theoretical value is correct *only* up to the order as the resultant theoretical expression Eq.(28) is heavily approximated at various levels.

It is also interesting to see the scaling law of this turbulence, which is shown in Fig.7. The energy-wave number scaling  $E_\omega \propto \omega^{-\kappa}$  ranges from a very steep slope with  $\kappa \sim 5.64$  to about  $\kappa \sim 1.92$ . For the scaling law (34), a probable set of parameters [please see Eq.(31)] comes out to be  $(\eta, \beta) \simeq (0.52, 0)$ . Similar scaling is also found to be obeyed in weakly ionized plasmas by other authors [43].

## B. Dust effects

We end this discussion by incorporating the effect of negatively charged dust particles on pinned solitons. This also supports our observation of the formation of pinned solitons as results of turbulence produced by counter-streaming ions as a response to negatively charged debris. We should however note that studying the effect of dust particles on the IICSI is *not* among our primary objectives. We include this section, just as a proof of concept and show that the simulation results are consistent with the present knowledge of dust effects on such solitons.

As shown in many other works [4], the presence of negatively charged dust particles increases the effective ion-sound speed of plasma making near-sonic events sub-sonic. In the limit of large-wavelength perturbation ( $k\lambda_D \gg 1$ ) and negligible ion temperature ( $\sigma \ll 1$ ), the IA dispersion relation becomes [4]

$$\omega \simeq k \left( \frac{n_{i0}}{n_{e0}} \right)^{1/2} c_s. \quad (44)$$

Note that in the presence of negative dust particles  $n_{i0}/n_{e0} > 1$  due to depletion of electrons and the overall effect can be viewed as an *effective* increase of sound speed  $c_{\text{effective}}$ , with

$$c_{\text{effective}} = \left( \frac{n_{i0}}{n_{e0}} \right)^{1/2} c_s. \quad (45)$$

This effect can be clearly seen in Fig.8, where we have included negatively charged dust particles. The dust particles are assumed to be cold and the number density is assumed to be constant at  $10^{12} \text{ m}^{-3}$ . The *h*-PIC-MCC code consistently takes the dust-charging as well as dust-charge fluctuation into account [19, 20]. In Fig.8, one can directly compare the corresponding results for zero-dust cases in Fig.3 (second and third panels from the top) where we see the reductions of amplitudes of pinned solitons for  $v_{\text{deb}} = 0.5$  and 1.0. Note that in the bottom panel of Fig.8, the increase of height of the soliton in the right is compensated by the decrease of height of the soliton in the left, making the total energy almost same.

## VI. SUMMARY AND CONCLUSIONS

In summary, we in this work, have considered an *e-i* plasma in the presence of an external, gaussian-shaped, charge perturbation (debris) moving through the plasma in an ion-acoustic time scale. We find that the response of the plasma differs significantly depending on the nature and the magnitude of debris charge density and its velocity. The simulation is being carried out with the well-tested *h*-PIC-MCC code [18-20], which can take into account dust and dust-charge fluctuation self-consistently. We have shown that while a positively charged external perturbation

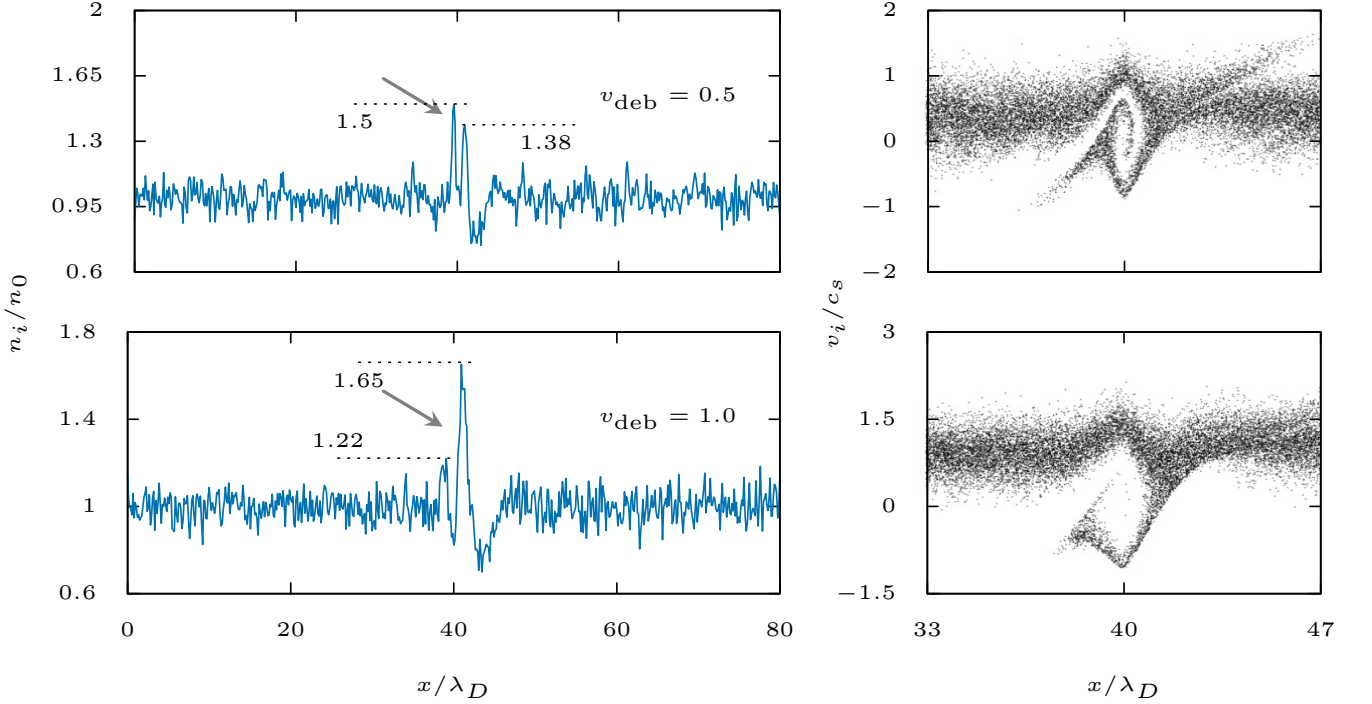


Figure 8. Effect of negatively charged dust particles on the amplitude of pinned solitons, corresponding to the same cases for  $v_{deb} = 0.5, 1.0$  (normalized by ion-sound speed  $c_s$ ) without any dust (see corresponding panels in Fig.3). The reduced amplitude of pinned solitons is clearly visible. Note that the equilibrium dust density is kept at 0.01% of the plasma density ( $n_{d0} \sim 10^{-4}n_0$ ) and in the bottom panel, the increase of height of the soliton in the right is compensated by the decrease of height of the soliton in the left, making the total energy almost same.

produces DSWs in the precursor region, a negatively charged perturbation causes an IICSI, which quickly becomes turbulent, giving rise to the pinned solitons. In the ion density plot as well as in the scatter plot of the ion phase-space for various debris velocities, we see that when debris velocity increases, it causes widening of the phase space vortices causing well-separated pinned solitons, which merge to form one single soliton when debris velocity reduces to zero. In the opposite extreme, when debris velocity becomes highly supersonic, the vortices are widened up to a limit causing the pinned solitons to disappear altogether.

We further show that as demonstrated through a linear analysis, the counter-streaming ions must exceed a critical velocity  $v_c$  in order for the IICSI to be excited, which in this case is directly related to the strength of negatively charged debris charge density  $\rho_{deb}$ , which causes the ions to counter stream. So, in order to have pinned soliton formation, the  $\rho_{deb}$  must be above a certain value. This value as determined from the simulation closely agrees with the analytical estimated value. Beyond this value of  $\rho_{deb}$ , the higher is the value of  $\rho_{deb}$ , the quicker the IICSI develops.

Through this work, we have shown that the pinned solitons are actually manifestation of the ion phase-space vortices formed in the turbulent regime of the ion-ion counter-streaming instability (IICSI), where ions are effectively trapped in the potential structure. Our simulation results are supported by the linear kinetic theory, through which we have shown the existence of critical debris charge density for the instability to turn turbulent. We have shown that a  $E_\omega \propto \omega^{-\kappa}$ , Kolmogorov-type energy cascading scaling [28, 43] exists in the turbulent regime which supports the formation of pinned solitons. In this context, we have the validity of MMT model in the case of 1D turbulence which also supports the scaling law for energy cascading. Toward the end, we have shown the effect of negatively charged dust particles on the pinned solitons, which causes the amplitude of the solitons to decrease and thus requires relatively large debris velocity to make the pinned solitons appear as compared to the case when there is no dust particle. These results largely agree with the fluid simulation results [4].

As a concluding remark, we would like to emphasize a bit about the future outlook of this work. We have already mentioned that through this work we have tried to look into the basic physics involving the fundamental problem of plasma interactions with embedded charged debris. Naturally, it is quite tempting to see whether these findings can be extrapolated toward certain applicability namely the detection of space debris. However, at this point, it is worth noting that the science of detection of space debris through possible plasma activities is still an open question and research in this direction is in a nascent stage. Though there are other theoretical works involving plasma interaction



with external charged debris [44], the scientific community as a whole, has not been able to detect such plasma activities so far, resulting out of space debris [45] and we need more insights into the problem including the effect of stochastic and periodic variations of cumulative charge of such debris on plasma waves, which are some possible interesting extensions to this work. Toward this, we believe this work provides a renewed look into the fundamental nature of such problems.

### ACKNOWLEDGEMENT

One of the authors MPB would like to acknowledge DST-SERB financial grant (CRG/2018/002971), India during which parts of this work related to the development of the simulation code *h*-PIC-MCC, was carried out. The authors would like to thank the anonymous referees for their constructive suggestions.

### APPENDIX A

The Boltzmann-Vlasov equation in the first-order perturbed distribution function is given by

$$\frac{\partial f_{j1}}{\partial t} + \mathbf{u}_j \cdot \nabla f_{j1} + \frac{q_j}{m_j} \mathbf{E}_1 \cdot \frac{\partial f_{j0}}{\partial \mathbf{u}_j} = 0. \quad (\text{A1})$$

Without loss of any generality, we assume the perturbation to be in  $\hat{\mathbf{x}}$  direction so that the perturbed VDF can be written as

$$f_{j1} = -\frac{iq_j}{m_j} E_{1x} \left( \frac{\partial f_{j0} / \partial u_j}{\omega - k u_j} \right), \quad (\text{A2})$$

where  $u_j \equiv \mathbf{u}_j \cdot \hat{\mathbf{x}}$ . Using the linearized Poisson's equation, we finally have

$$\epsilon_0 \nabla \cdot \mathbf{E}_1 = \sum_j q_j n_{j1}, \quad (\text{A3})$$

where  $n_{j1}$  is the perturbed number density of the  $j$ th species, expressed as a *fluid* quantity, through the perturbed VDF,

$$n_{j1} = \int f_{j1} d\mathbf{u}_j, \quad (\text{A4})$$

where the integration has to be carried over the 3-dimensional velocity space.

We now write the VDF  $f_j$  in terms of the unit-normalized VDF  $\hat{f}_j$ , so that

$$f_{j0} \equiv n_{j0} \hat{f}_{j0}. \quad (\text{A5})$$

The one-dimensional normalized VDF for  $j$ th species can be written as

$$\hat{f}_{j0}(u) = (2\pi c_j^2)^{-1/2} \exp \left[ -\frac{(u - v_j)^2}{2c_j^2} \right], \quad \int \hat{f}_{j0} d\mathbf{u} = 1. \quad (\text{A6})$$

Substituting all the expressions in the perturbed Poisson's equation, Eq.(A3), we finally arrive at the linear dispersion equation

$$k^2 - \sum_j \omega_{pj}^2 \int_{-\infty}^{+\infty} \frac{\hat{f}'_{j0}}{u_j - \omega/k} du_j = 0, \quad (\text{A7})$$

where  $\omega_{pj}$  is the plasma frequency of the  $j$ th species and

$$\hat{f}'_{j0} = \frac{\partial \hat{f}_{j0}}{\partial u_j}. \quad (\text{A8})$$



We know that the integral in the above dispersion relation is singular, which leads to the well-known Landau damping term in a plasma with no equilibrium drift velocities. In any case, the singular integral can be evaluated approximately assuming that the singularity lies very close to the real  $u$ -axis [30]. Decomposing the integral into a non-singular part in terms of Cauchy principal value integration and the approximating singular part through residue theorem, we have,

$$\int_{-\infty}^{+\infty} \frac{\hat{f}'_{j0}}{u_j - \omega/k} du_j \simeq \mathbb{P} \int_{-\infty}^{+\infty} \frac{\hat{f}'_{j0}}{u_j - \omega/k} du_j + i\pi \hat{f}'_{j0} \Big|_{u_j=\omega/k}, \quad (\text{A9})$$

where  $\mathbb{P}$  indicates the principal value integration. The final dispersion relation is now given as

$$k^2 - \sum_j \omega_{pj}^2 \left( \mathbb{P} \int_{-\infty}^{+\infty} \frac{\hat{f}'_{j0}}{u_j - \omega/k} du_j + i\pi \hat{f}'_{j0} \Big|_{u_j=\omega/k} \right) = 0. \quad (\text{A10})$$

## APPENDIX B

The principal value integrations given in Eq.(25) can be found out to be

$$\mathbb{P} \int_{-\infty}^{+\infty} \frac{F'(u)}{u - \tilde{\omega}^+/k} du \simeq \frac{k^2}{(\omega + kv/2)^2} \langle (1 - ku/\tilde{\omega}^+)^{-2} \rangle, \quad (\text{B1})$$

$$\mathbb{P} \int_{-\infty}^{+\infty} \frac{F'(u)}{u - \tilde{\omega}^-/k} du \simeq \frac{k^2}{(\omega - kv/2)^2} \langle (1 - ku/\tilde{\omega}^-)^{-2} \rangle, \quad (\text{B2})$$

where  $\tilde{\omega}^\pm/k$  are the phase velocities. The angular brackets indicate the average of the quantity with respect to the equilibrium VDFs  $F(u)$ . The quantities inside the  $\langle \rangle$  provide the correction terms to the ion-plasma oscillation frequency and to the first order, which can be neglected if we ignore its effect on counter-streaming instability. Approximating  $\langle \rangle \sim 1$ , we have

$$\left( 1 + \frac{1}{k^2 \lambda_{De}^2} \right) - i\pi \frac{1}{2k^2} \omega_{pi}^2 \left( \frac{\partial F}{\partial u} \Big|_{u=\tilde{\omega}^+/k} + \frac{\partial F}{\partial u} \Big|_{u=\tilde{\omega}^-/k} \right) \simeq 2 \frac{\omega_{pi}^2}{\omega^2} \left[ \frac{1}{(2 + kv/\omega)^2} + \frac{1}{(2 - kv/\omega)^2} \right]. \quad (\text{B3})$$

Multiplying the whole equation by  $\omega^2$  and thereafter approximating  $\omega \sim \omega_{pi}$  on the right hand side, we can simplify the above equations as

$$\omega^2 \simeq 2\alpha \omega_{pi}^2 \tilde{\omega}_{pi}^2 \left[ 1 - i\pi \frac{1}{2k^2} \alpha \omega_{pi}^2 \left( \frac{\partial F}{\partial u} \Big|_{u=\tilde{\omega}^+/k} + \frac{\partial F}{\partial u} \Big|_{u=\tilde{\omega}^-/k} \right) \right]^{-1} \quad (\text{B4})$$

where

$$\alpha = \left( 1 + \frac{1}{k^2 \lambda_{De}^2} \right)^{-1}, \quad (\text{B5})$$

$$\tilde{\omega}_{pi}^2 = \frac{1}{(2 + kv/\omega_{pi})^2} + \frac{1}{(2 - kv/\omega_{pi})^2} \quad (\text{B6})$$

For small  $\text{Im}(\omega)$ , one can expand the above expression to get an expression for the growth rate as

$$\text{Im}(\omega) \simeq \pi \left( \frac{\alpha}{2} \right)^{3/2} \frac{\omega_{pi}^3}{k^2} \tilde{\omega}_{pi} \left( \frac{\partial F}{\partial u} \Big|_{u=\tilde{\omega}^+/k} + \frac{\partial F}{\partial u} \Big|_{u=\tilde{\omega}^-/k} \right). \quad (\text{B7})$$

We note that

$$\frac{\partial F}{\partial u} \Big|_{u=\tilde{\omega}^+/k} = -\frac{(\omega/k + v/2)}{c_i^3 \sqrt{2\pi}} \exp \left[ -\frac{(\omega/k + v/2)^2}{2c_i^2} \right], \quad (\text{B8})$$

$$\frac{\partial F}{\partial u} \Big|_{u=\tilde{\omega}^-/k} = -\frac{(\omega/k - v/2)}{c_i^3 \sqrt{2\pi}} \exp \left[ -\frac{(\omega/k - v/2)^2}{2c_i^2} \right], \quad (\text{B9})$$

so that the growth rate of the instability can be approximated as

$$\begin{aligned} \text{Im} \left( \frac{\omega}{\omega_{pi}} \right) \simeq & \frac{1}{4} \sqrt{\alpha^3} \pi \left( \frac{\omega_{pi}}{kc_i} \right)^3 \tilde{\omega}_{pi} \left\{ \left( \frac{kv}{2\omega_{pi}} - 1 \right) \exp \left[ -\frac{(\omega_{pi} - kv/2)^2}{2k^2 c_i^2} \right] \right. \\ & \left. - \left( \frac{kv}{2\omega_{pi}} + 1 \right) \exp \left[ -\frac{(\omega_{pi} + kv/2)^2}{2k^2 c_i^2} \right] \right\}, \end{aligned} \quad (\text{B10})$$

where we have set  $\omega \sim \omega_{pi}$  on the right hand side.

- 
- [1] Sen A, Tiwari S, Mishra S, Kaw P. Adv Space Res. 2015;56(3):429.
- [2] Tiwari SK, Sen A. Phys Plasmas. 2016;23:100705.
- [3] Kumar A, Sen A. New J Phys. 2020;22:073057.
- [4] Sarkar H, Bora MP. Phys Plasmas. 2023;30:083701.
- [5] Arora G, Bandyopadhyay P, Hariprasad MG, Sen A. Phys Rev E. 2021;103(013201).
- [6] Jaiswal S, Bandyopadhyay P, Sen A. Phys Rev E. 2016;93:041201(R).
- [7] Arora G, Bandyopadhyay P, Hariprasad MG, Sen A. Phys Plasmas. 2019;26(093701).
- [8] Neufeld J, Ritchie RH. Phys Rev. 1955;98:1632.
- [9] Hutchinson IH. Phys Plasmas. 2011;18:032111.
- [10] Block D, Carstensen J, Ludwig P, Miloch WJ, Greiner F, Piel A, et al. Contrib Plasma Phys. 2012;52(10):804.
- [11] Ali S, Khan S. Phys Plasmas. 2013;20:072106.
- [12] Malka V. Phys Plasmas. 2012;19:055501.
- [13] Wang R, Vasko IY, Mozer FS, Bale SD, Artemyev AV, Bonnell JW, et al. Astrophys J Lett. 2020;889:L9.
- [14] Khusroo M, Bora MP. Phys Rev E. 2019;99:013205.
- [15] Schamel H. Phys Rep. 1986;140:161.
- [16] Vasko IY, Mozer FS, Krasnoselskikh VVea. Gephys Res Lett. 2018;45:5809.
- [17] Burch JL, Moore TE, Torbert RB, Giles BL. Space Sci Rev. 2016;199:5.
- [18] Changmai S, Bora MP. Phys Plasmas. 2019;26(042113).
- [19] Changmai S, Bora MP. Sci Rep. 2020;10:20980.
- [20] Das M, Changmai S, Bora MP. Phys Rev E. 2023;108:045202.
- [21] Jackson JD. J Nucl Energy, Part C Plasma Phys. 1960;1:171.
- [22] Forslund DW, Shonk CR. Phys Rev Lett. 1970;25(5):281.
- [23] Stringer TE. J Nucl Energy, Part C Plasma Phys. 1964;6:267.
- [24] Rose DV, Genoni TC, Welch DR, Startsev EA, Davidson RC. Phys Rev ST Accel Beams. 2007;10(034203).
- [25] Dieckmann ME, Drury LO, Shukla PK. New J Phys. 2006;8:40.
- [26] Smith DF, Fung PCW. J Plasma Phys. 1971;5(1):1.
- [27] Kiwamoto Y. J Phys Soc Jpn. 1974;37(2):466.
- [28] Kolmogorov AN. Comptes Rendus de l'Academie Des Sciences de l'URSS. 1941;16:32.
- [29] Chapman T, Winjum BJ, Berger RL, Dimits A, Banks JW, Brunner S, et al. Phys Plasmas. 2021;28:022105.
- [30] Chen FF. Introduction to plasma physics and controlled fusion. vol. 1. 2nd ed. Plenum Press, New York and London; 1974.
- [31] Birdsall CK, Langdon AB. Plasma Physics via Computer Simulation. CRC Press; 2004.
- [32] Perek L. Space Debris. 2000;2:123.
- [33] Garrett HB. Rev Geophys. 1981;19(4):577.
- [34] Whipple EC. Rep Prog Phys. 1981;44:1196.
- [35] Havnes O, Aanesan TK, Melandsø F. J Geophys Res. 1990;89:6581.
- [36] Goree J. Plasma Sources Sci Technol. 1994;3:400.
- [37] Juhasz A, Horanyi M. J Geophys Res. 1997;102(A4):7237.
- [38] Anderson PC. J Geophys Res. 2012;117:A07308.
- [39] Mandell MJ, Davis VA, Davis GT, Maurer RH, Herrmann C. IEEE Trans Plasma Sci. 2012;40(2):209.
- [40] Vaulina OS, Nefedov AP, Petrov OF, Krapak SA. J Exp Theor Phys. 1999;88:1130.
- [41] Majda AJ, McLaughlin DW, Tabak EG. J Nonlinear Sci. 1997;6:9.
- [42] Zakharov VE, Guyenne P, Pushkarev AN, Dias F. Physica D. 2001;152-153:573.
- [43] Krishan V, Yoshida Z. Mon Not R Astron Soc. 2009;395(4):2039.
- [44] Truitt AS, Hartzell CM. J Spacecr Rockets. 2020;57(5):975.
- [45] Bernhardt PA, Scott L, Howarth A, Morales GJ. Phys Plasmas. 2023;30:092106.